PCCP

Cite this: *Phys. Chem. Chem. Phys.*, 2012, **14**, 2934–2939

www.rsc.org/pccp

PAPER

Improved kinetics of $LiNi_{1/3}Mn_{1/3}Co_{1/3}O_2$ cathode material through reduced graphene oxide networks†

Ke-Cheng Jiang,[ac] Sen Xin,[ac] Jong-Sook Lee,[b] Jaekook Kim,[b] Xiao-Ling Xiao[c] and Yu-Guo Guo*[ab]

Received 25th October 2011, Accepted 15th December 2011
DOI: 10.1039/c2cp23363k

An electronically conducting 3D network of reduced graphene oxide (RGO) was introduced into $LiNi_{1/3}Mn_{1/3}Co_{1/3}O_2$ (LNMC) cathode material in a special nano/micro hierarchical structure. The rate test and cycling measurement showed that the hierarchical networks remarkably improve the high rate performance of LNMC electrode for lithium-ion batteries. The effect of RGO conducting networks on kinetic property was investigated by electrochemical impedance spectroscopy (EIS) and potentiostatic intermittent titration (PITT). The EIS results reveal that the RGO network greatly decreases the resistance of lithium batteries, especially the charge transfer resistance which can be attributed to the significantly improved conducting networks. The enhancement of apparent diffusion coefficient by the RGO conducting networks is shown by PITT. The power performance was found to be limited by the electrical conduction in the two-phase region, which can be greatly facilitated by the hierarchical RGO network together with carbon black. The as-obtained LNMC/RGO cathode exhibits an outstanding electrochemical property supporting the design idea of electronically conducting 3D networks for the high-energy and high-power lithium-ion batteries.

1. Introduction

Because of easy synthesis and good cycling stability, $LiCoO_2$ has been used in commercial lithium-ion batteries as the cathode material from the 1990s.[1–3] Nonetheless, the attainable rechargeable capacity of $LiCoO_2$ is only about 140 mA h g^{-1} (50% of the theoretical capacity) limited by its structure stability.[4,5] Furthermore, cobalt is expensive and environmentally unfriendly. Therefore intensive effort has been put in exploiting alternative cathode materials.[6–9]

Among the candidates, $LiNi_{1/3}Mn_{1/3}Co_{1/3}O_2$ (LNMC), which was first reported by Ohzuku's group,[10] has attracted a lot of interest. As a member of the multicomponent solid solution family, LNMC exhibits high energy density, stable structure, improved safety and low cost due to the synergistic effect of transition metal ions.[11–13] However, the cation disorder occurred during calcination causes a fraction of Li ions to enter 3b sites of transition-metal instead of the normal 3a sites, leading to the deterioration in the kinetic property which decides the high-rate performance.[14] To enhance the electrochemical property especially the kinetic capability, tremendous effort has been made which include: (i) Partially substituting LNMC with foreign atoms (Sn,[15] Si[16]), through which the structural stability and cycle performance may be improved. However, introducing guest atoms into the crystal lattices of LNMC may also cause a lowering of capacity because the substituents are usually electrochemically inactive, (ii) Surface coating with metal oxide materials (Al_2O_3,[17] ZrO_2,[18] ZnO[19]) has also been widely used for improving the high rate performance of poor kinetic electrode materials. However, perfect surface coatings and desired mixtures are often very difficult to achieve, hence the power-performance enhancement of such electrode materials is still limited. (iii) Decreasing the particle size may also improve the transport issues. According to the diffusion formula $\tau = L^2/2D$ where τ is the diffusion time, L is the diffusion distance, and D is the diffusion coefficient, reducing the particle size can significantly shorten the diffusion time of Li in LNMC, resulting in a much enhanced power performance. However, nanometre-sized LNMC usually exhibits a poor cycling performance,[20] low tap density,[21] and there are also handling problems in admixing with carbon black and electrode preparation.

An optimized nanostructure design to overcome the kinetic limitation is mixed conducting 3D networks,[22–25] which means a nanometre-sized network composed of active materials and

[a] *Beijing National Laboratory for Molecular Sciences (BNLMS), Institute of Chemistry, Chinese Academy of Sciences (CAS), Beijing 100190, P.R. China. E-mail: ygguo@iccas.ac.cn; Fax: +86-10-62557908; Tel: +86-10-62557908*
[b] *School of Materials Science and Engineering, Chonnam National University (WCU), Gwangju 500-757, Republic of Korea*
[c] *Graduate University of Chinese Academy of Sciences, Beijing 100049, P.R. China*

† Electronic supplementary information (ESI) available: Raman spectrum and SEM image of RGO, and SEM image of cross-sectional view of the RGO-free LNMC electrode. See DOI: 10.1039/c2cp23363k

paths for both lithium ions and electrons, together with a microscopic conductive network superimposed on the nanoscopic network and carbon black. While the nanometre-sized network can reduce the effective diffusion length to a few nanometres leading to negligible diffusion times, the microscopic network can increase the conductive contact between nanometre-sized active particles and the current collector, and improve the overall electrical conductivity remarkably. It has been demonstrated that some carbon-based materials, such as carbon nanotubes,[26] carbon nanofibers[27] and porous carbon,[28] can construct an efficient mixed conducting 3D network during the preparation of anode materials. However, thermal treatment for the *in situ* preparation of nanoscopic carbon network in anode materials cannot be applied to cathode materials since the oxide cathode material may be reduced during the synthesis process.

Graphene and reduced graphene oxide (RGO) have attracted considerable attention for many applications in recent years.[29–31] Due to their extraordinary electronic behavior, stable chemical property, excellent mechanical properties, and high specific surface area,[32–34] it is suggested that they can be promising materials for constructing 3D conducting networks by a suitable mixing procedure.[35,36] Recently, RGO nanosheets and their composites have been intensively investigated as electrode materials for lithium-ion batteries and excellent performances have been observed.[37–42] However, the trend of adding RGO to materials is limited with guidance of theory and deep study. In this work, we tried to further describe the effect of nanostructure materials containing RGO on charge transfer mechanisms of electrode materials.

2. Experimental section

The LNMC powders were synthesized by a sol–gel method using citric acid as the chelating agent.[11,43,44] A stoichiometric amount of lithium acetate, manganese acetate, nickel acetate and cobalt acetate were chosen as starting materials to prepare the precursor. All salts were dissolved in distilled water and added drop-wise into citric acid solution with continuous stirring. After the dissolution of all salts, the temperature of solution was raised to 80 °C. Continued stirring was applied until the clear viscous gel was formed. The gel was dried in an oven at 100 °C to obtain the precursor powder. After precalcining at 450 °C in air for 5 h, the powder was grounded and pelletized and then calcined at 900 °C for 12 h in air.

In order to get well dispersed RGO, natural graphite was oxidized using a modified Hummers method[38,45] followed with reducing in H_2/Ar stream. At first, 2g graphite was poured into 50 mL of concentrated H_2SO_4 with 1g $NaNO_3$, and the mixture was cooled down to 0 °C. Then, 6 g $KMnO_4$ were added slowly while maintaining the temperature below 5 °C. The cooling bath was removed and the suspension was maintained quiescent by 90 min. After that, 100 mL of water was added and the temperature was increased to 90 °C. The mixture was further diluted with 300 mL of water, treated with 50 mL of 5% H_2O_2, filtered and washed with hot water. After being dried in vacuum, the graphene oxide was reduced under H_2/Ar flowing condition for 2 h. The production was mixed with *N*-methyl-pyrrolidinone (NMP) by vigorous ultrasonication for 8 h to obtain a well dispersed RGO/NMP suspension.

To prepare the electrode with mixed conducting 3D networks, a mixture of LNMC, RGO/NMP suspension, carbon black (CB), and poly(vinyl difluoride) (PVDF) at a weight ratio of 80 : 5 : 5 : 10 was pasted on an Al foil. For comparison, a mixture of LNMC, CB, and PVDF at a weight ratio of 80 : 10 : 10 was also prepared.

X-ray diffraction (XRD) measurements of the LNMC powder were carried out using a Philips PW3710 with filtered Cu-Kα radiation (Rigaku D/max-2500). A scanning electron microscope (SEM) (JEOL 6701F, operating at 10kV) was employed to investigate the morphology of the LNMC powders and the electrode films.

Electrochemical measurements were performed using Swagelok-type cells assembled in an argon-filled glove box. Pure lithium foil was used as a counter electrode. A glass fiber (GF/D) from Whatman was used as the separator. The electrolyte consisted of a solution of 1 M $LiPF_6$ in ethylenecarbonate (EC)/dimethylcarbonate (DMC)/diethylcarbonate (DEC) (1 : 1 : 1, in wt%) obtained from Tianjing Jinniu Power Sources Material Co. Ltd. Galvanostatic cycling of the assembled cells was carried out using an Arbin BT2000 system in the voltage range of 2.5–4.3 V (*vs.* Li^+/Li). Cyclic voltammetry (CV), electrochemical impedance spectroscopy (EIS) and potentiostatic intermittent titration technique (PITT) measurements were carried out on an Autolab PG302N.

3. Results and discussion

Fig. 1a shows the XRD pattern and Rietveld refinement results of the as-obtained LNMC. The results reveal that the LNMC has a typical layered structure of α-$NaFeO_2$ type with space group $R\bar{3}m$. The structure consists of a cubic close-packed arrangement of oxide ions. The transition metal ions in the structure occupy alternating layers in the octahedral sites. The hexagonal lattice parameters are determined to be a = 0.28629 nm, c = 1.42408 nm, and volume = 0.101083 nm^3, with 5.93% Ni^{2+} ions migrating to the lithium sites (Rp = 8.55%, Rwp = 12.4%), indicating a low degree of cation disorder in the structure.[46] Fig. 1b shows the XRD patterns of the natural graphite, the graphene oxide and the RGO. It can be noted that after reduction by H_2/Ar air the broad (002) peak shifted to 25.5° from 12.46°. The result indicates the formation of RGO from graphene oxide,[9] which is further confirmed by the Raman spectrum (see Fig. S1 in ESI†).

A typical SEM image of the LNMC particles synthesized by the sol–gel process is shown in Fig. 2a. It can be clearly seen that the as-synthesized LNMC powders exhibit uniform size with smooth facets, which indicates their high crystallinity. In the RGO-free LNMC electrode, wide interspaces between LNMC particles and CB are found, and the CB itself cannot form interconnected network, which might lead to limited kinetics of the electrode (see Fig. S2 in ESI†). However, after introducing RGO into the electrode, the weak point is released as shown in the SEM images of a cross-sectional view of the RGO-added LNMC electrode (Fig. 2c,d). The LNMC particles are well mixed with RGO and CB (*ca.* 50 nm) without the wide interspaces. Due to the excellent electrical conductivity and the special two-dimensional (2D) structure (see Fig. S3 in ESI†), the RGO nanosheets form a 3D interconnected network over the

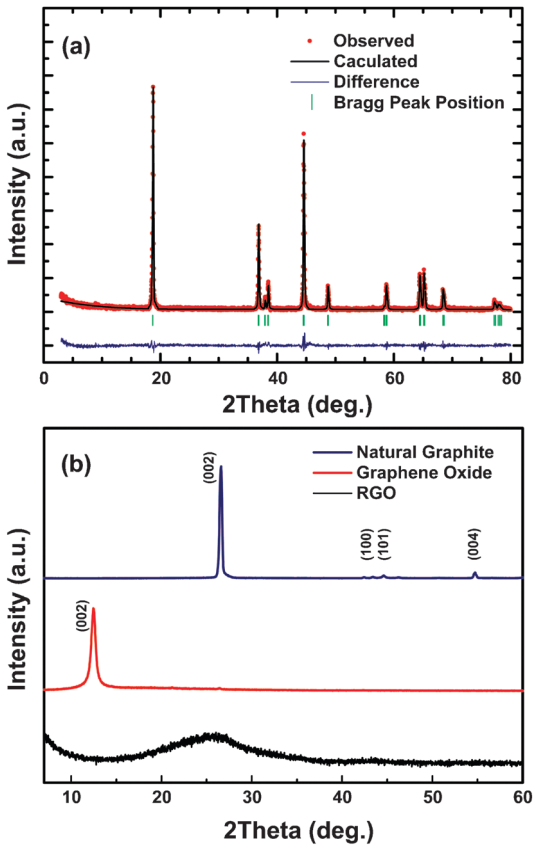

Fig. 1 (a) Rietveld refinement and XRD pattern of LNMC. (b) XRD patterns of natural graphite, graphene oxide and RGO.

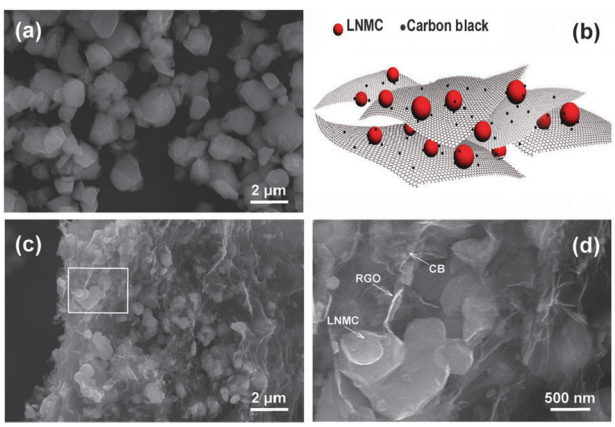

Fig. 2 (a) SEM image of LNMC particles, (b) schematic illustration of the 3D networks formed by the LNMC, RGO and CB, (c) SEM image of a cross-sectional view of the RGO-added LNMC electrode, (d) high-magnification SEM image of the selected area in (c).

LNMC particles and the CB particles as illustrated in Fig. 2b. The 3D conducting network, together with CB, is expected to provide sufficient electrons from the Cu foil current collector for the storage of Li in each LNMC particles and hence to improve the kinetics (Fig. 2c,d).[23]

CV measurements were made to study the effect of RGO on the LNMC cathode (Fig. 3). CV curves were recorded over the potential range of 2.5–4.3 V at a scan rate of 0.2 mV s^{-1} for the first three cycles. After the addition of RGO, it can be seen that the oxidation and reduction peaks become closer, the peak width is narrowed and the peak current intensity is increased. The results indicate that the polarization of the LNMC electrode has been reduced by RGO. Improved kinetic properties of the RGO-added LNMC cathode can be expected.

To examine kinetics performance of the RGO-free and the RGO-added LNMC electrodes, the cells were cycled at different C-rates (Fig. 4a) between 2.5–4.3 V *vs.* Li^+/Li. For all rates tested from 0.1C to 20C (1C = 170 mA g^{-1}), the RGO-added LNMC electrode exhibits a higher specific capacity than the RGO-free one. While the RGO-free electrode exhibits nearly no capacity at 6C, the RGO-added one can still deliver a charge/discharge capacity of larger than 110 mA h g^{-1}. The capacity retains at as high as 55 mA h g^{-1} even at 20C. Fig. 4b shows the excellent cycling behavior of the RGO-added LNMC electrode cycled at 1C for 100 cycles, in which only a very tiny decrease is observed in the specific capacity. The Coulombic efficiencies (calculated from the discharge capacity/charge capacity) of the RGO-added electrode are always stabilized at 99–100% after the first cycle. The excellent high rate capability and long term cyclability demonstrate that the 3D conducting network constructed by RGO can effectively enhance the kinetics of LNMC.

The effect of RGO on the LNMC electrode is further confirmed by EIS and PITT measurements. EIS measurements were carried out by applying an AC signal of 10 mV amplitude over the frequency range from 0.5 Hz to 100 kHz. For the PITT measurements, a potential step of 10 mV was applied and the current was recorded as a function of time. A PITT measurement was made after an EIS, and then the cells were charged at a current density of 6.75 mA g^{-1} for 30 min to reach the next charge state for measurements, followed by open circuit relaxation for 5 h. The process was repeated continuously until the voltage of the cell reached 4.3 V.

Fig. 5 compares the EIS spectra of the RGO-free and RGO-added LNMC electrodes at various states of charge, with equivalent circuits shown in insets. In the equivalent circuit, R_u is the uncompensated ohmic resistance of the electrodes, representing

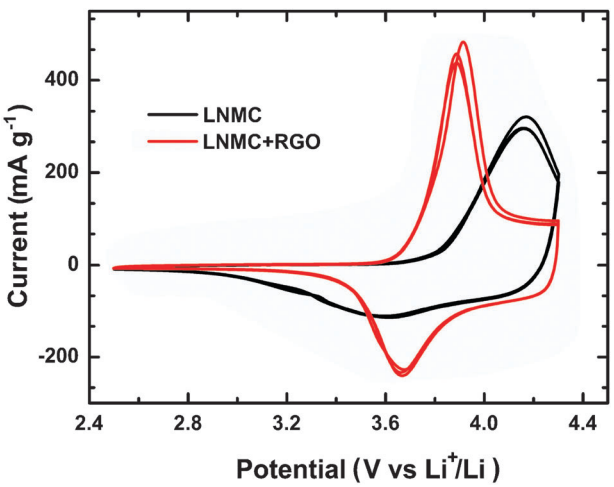

Fig. 3 Cyclic voltammograms for the RGO-free and RGO-added LNMC electrodes at a scan rate of 0.2 mV s^{-1}.

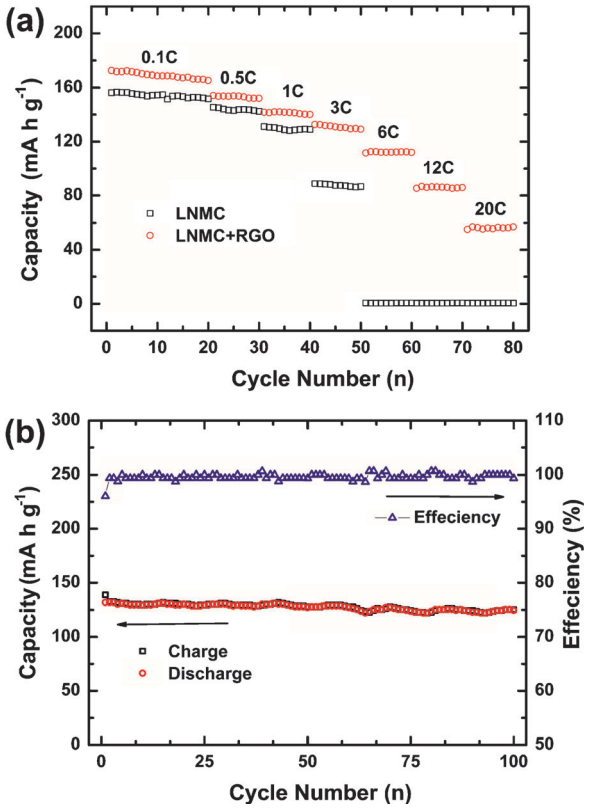

Fig. 4 (a) Rate performance of the RGO-free and RGO-added LNMC electrodes in the voltage range of 2.5–4.3 V *vs.* Li^+/Li. (b) Cycle performance of the RGO-added LNMC electrode cycled at 1C.

the ohmic polarization. Except the initial state of $x = 0$, all the EIS spectra show two semicircles. The first semicircles at high frequency represented by a resistor R_s and a constant phase element CPE_s corresponding to the lithium ion transfer through the surface layer, while the second semicircles at lower frequency can be attributed to the charge transfer reaction represented by R_{ct} and the non-ideal double layer capacitance CPE_{dl}.[8] The values of parameters R_u, R_s and R_{ct} obtained by the nonlinear least squares fitting are summarized in Table 1. It can be seen that the addition of RGO decreases all the values of R_u, R_s and R_{ct}. Especially the R_{ct} is reduced markedly due to the improved electrical conductivity, indicating an enhancement in the kinetics and the consequent increase in high rate capability.

Fig. 6 reports the open circuit voltage (OCV) as a function of the composition of x in $Li_{1-x}Ni_{1/3}Mn_{1/3}Co_{1/3}O_2$ for the RGO-free and the RGO-added electrodes. Though both curves display a plateau at about 3.75 V representing the two-phase coexistence, the curve for the RGO-added electrode is more extended which is consistent with the higher capacity shown by the cycling tests.

PITT has been used to determine the chemical diffusion coefficient based on Fick's law.[47] The equation for D_{app} measured by PITT can be expressed by eqn (1) for the time domain $t > r^2/D_{app}$:[48]

$$I = (2nFS\Delta C/r)\exp[(-\pi^2 D_{app}/4r^2)t] \quad (1)$$

where r is the radius of the single crystal particle, n is the charge transfer number, F is the Faraday constant, S is the

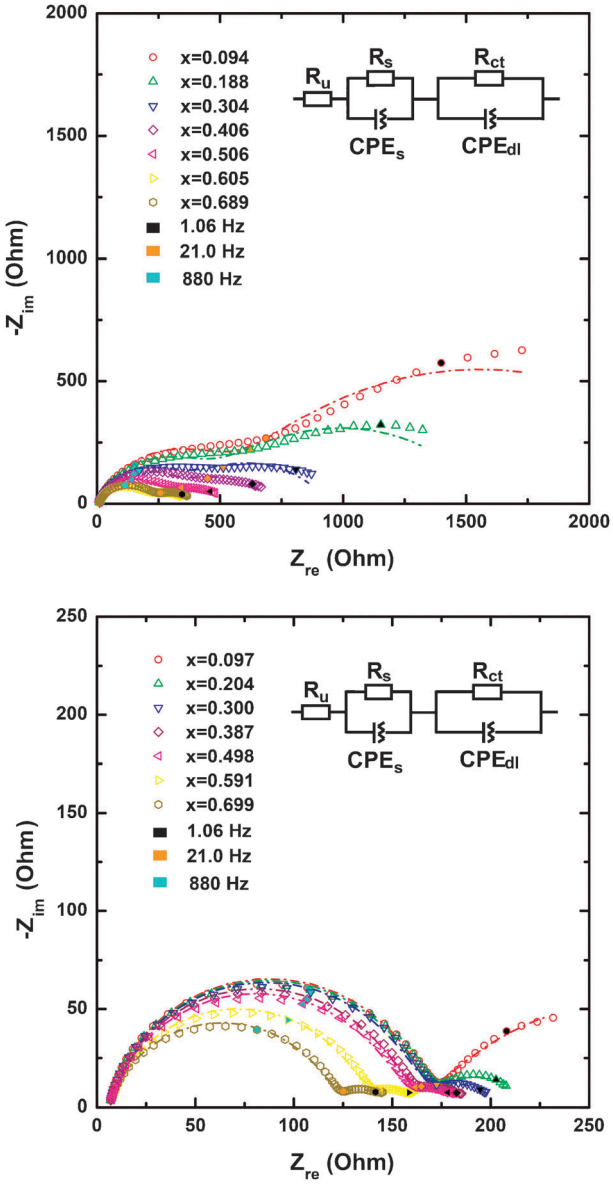

Fig. 5 EIS of (a) RGO-free LNMC electrode and (b) RGO-added LNMC electrode at various x in $Li_{1-x}Ni_{1/3}Mn_{1/3}Co_{1/3}O_2$ during charging.

geometric surface area of the particle, and ΔC is the variation of lithium concentration in the particle during the potential step. Eqn (1) can be rewritten as:

$$D_{app} = (-4r^2/\pi^2)(d\ln I/dt) \quad (2)$$

under the following assumptions:[49,50] (i) The current is controlled by Li ion diffusion in the solid. (ii) The particles are single crystal and there is no phase transformation during the Li ion extraction and insertion. (iii) The particles are uniform spheres and the diffusion length is the radius of the particles.

The D_{app} which was calculated from the slope of $\ln|I| - t$ curves is displayed in Fig. 7. The values are indicated by apparent diffusion coefficient, D_{app}, since the assumptions are not available in the present case. The cusp in the diffusivity curve of about one order of magnitude might be ascribed to

Table 1 Kinetic parameters obtained from equivalent circuit fitting of experimental data for the RGO-free and the RGO-added LNMC electrodes at various x in $Li_{1-x}Ni_{1/3}Mn_{1/3}Co_{1/3}O_2$[a]

LNMC				LNMC + RGO			
x	R_u/Ohm	R_s/Ohm	R_{ct}/Ohm	x	R_u/Ohm	R_s/Ohm	R_{ct}/Ohm
0.094	6.93 (0.62)	484 (58)	2152 (347)	0.097	5.75 (0.091)	161 (1.7)	212 (61)
0.188	6.88 (0.60)	408 (55)	1191 (148)	0.204	5.88 (0.093)	159 (2.4)	57.6 (8.4)
0.304	7.33 (0.56)	316 (44)	619 (73)	0.300	5.97 (0.10)	156 (3.2)	43.6 (7.3)
0.406	7.69 (0.46)	297 (32)	396 (47)	0.387	6.02 (0.11)	148 (3.3)	37.3 (6.6)
0.506	7.50 (0.36)	259 (29)	241 (19)	0.498	6.10 (0.15)	145 (4.3)	35.6 (8.4)
0.605	6.80 (0.33)	176 (13)	192 (20)	0.591	6.00 (0.14)	128 (3.4)	34.8 (7.8)
0.689	7.17 (0.26)	198 (10)	192 (19)	0.699	5.79 (0.12)	113 (2.6)	35.7 (7.4)

[a] The error values are shown in the brackets.

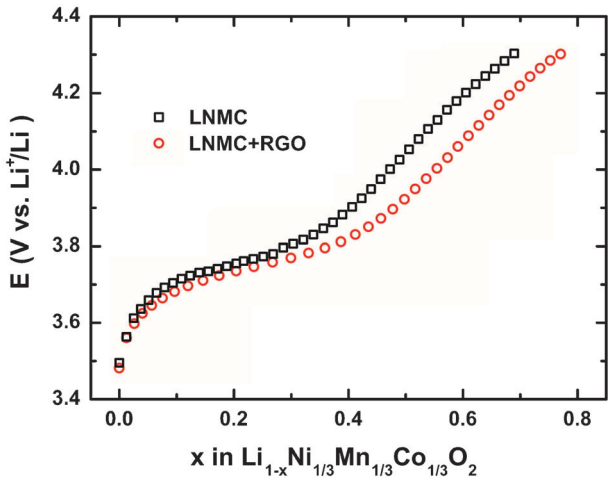

Fig. 6 Open circuit voltage (OCV) for the RGO-free and RGO-added LNMC electrode as a function of the composition x in $Li_{1-x}Ni_{1/3}Mn_{1/3}Co_{1/3}O_2$.

the phase transformation kinetics in the two-phase region. Similar but much stronger effects have been reported in the electrode material with narrow solubility and in the investigation using galvanostatic intermittent titration technique (GITT).[48,51,52] The PITT method employed in the present work suffers less from the phase transition and thus can be considered more reliable in the diffusivity determination than GITT which is usually based on the short time behavior.[48,50–52] The long time behavior under potentiostatic, constant driving force condition, eqn (1) is more likely to represent solid state diffusion by Fick's law even with the presence of the significant influence of the interfacial polarization as indicated in Fig. 5 (against assumption (i)) and even in the presence of the phase transition (against the assumption (ii)), as long as the phase transformation is controlled by solid state diffusion.

It can be seen that the added RGO markedly increases the apparent kinetics in the two-phase region, *i.e.* in the composition range of $0.05 < x < 0.4$ (Fig. 7a) and the voltage range of $3.6\ V < E < 4.0\ V$ (Fig. 7b). It is suggested that the phase transformation is greatly facilitated by the electrical transport provided by the RGO network. The results suggest that the phase transformation by lithium insertion/extraction is rather limited in two-phase nano-composites due to the poor electrical conduction, while the ionic conduction may be enough or less affected benefiting from the nano-sized active particles.

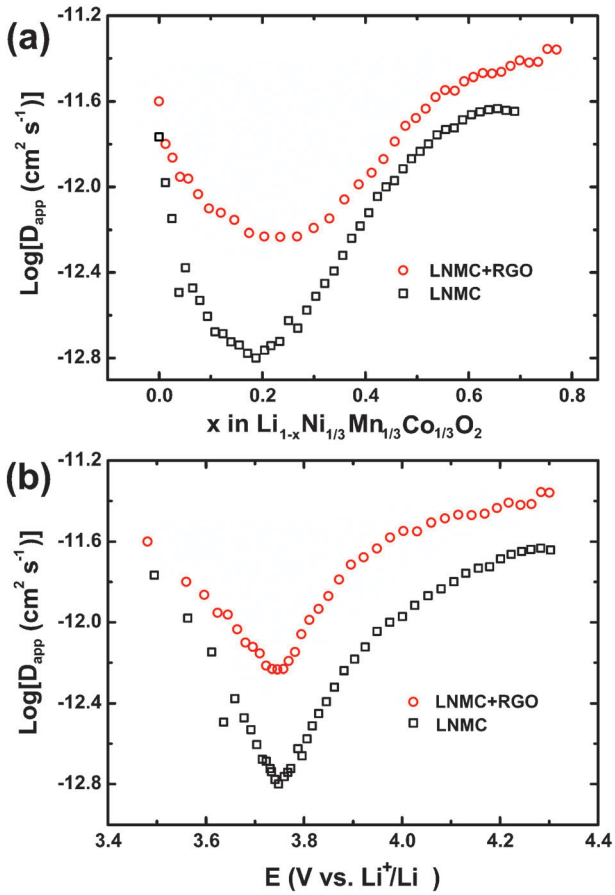

Fig. 7 Apparent chemical diffusion coefficient (D_{app}) of the Li ion in the RGO-free and RGO-added LNMC electrodes at (a) various composition x in $Li_{1-x}Ni_{1/3}Mn_{1/3}Co_{1/3}O_2$, and (b) various potentials.

4. Conclusions

3D conducting networks of RGO nanosheets have been introduced into LNMC cathodes in this work. Due to the special 2D structure and the excellent electrical conductivity, the RGO nanosheets provides high-speed electrical channels which can extend in a long distance for LNMC and carbon black. The rate and cycling tests demonstrate that such structure can significantly enhance the rate capability and long term cycling performance of LNMC. The EIS and PITT measurements confirm that the kinetics is substantially improved by the addition of RGO. Furthermore, the results reveal that the

rate performance is improved specifically in the two-phase region by the enhanced electrical conductivity benefiting from RGO networks. The 3D conducting networks in different design forms may also be effective for other electrode materials, used for advanced energy storage devices such as lithium ion batteries, supercapacitors, or hybrid with both high-power and high-energy densities.

Acknowledgements

This work is supported by the National Natural Science Foundation of China (No. 91127044 and 21121063), the National Key Project on Basic Research (Grant Nos. 2011CB935700 and 2009CB930400), the WCU program through NRF funded by MEST (R32-2009-000-20074-0), and the Chinese Academy of Sciences. The authors thank Prof. Hong Li and Prof. Zhongbo Hu for discussions.

Notes and references

1 K. Mizushima, P. Jones, P. Wiseman and J. Goodenough, *Mater. Res. Bull.*, 1980, **15**, 783–789.
2 B. L. Ellis, K. T. Lee and L. F. Nazar, *Chem. Mater.*, 2010, **22**, 691–714.
3 M. Okubo, E. Hosono, J. Kim, M. Enomoto, N. Kojima, T. Kudo, H. Zhou and I. Honma, *J. Am. Chem. Soc.*, 2007, **129**, 7444–7452.
4 J. N. Reimers and J. R. Dahn, *J. Electrochem. Soc.*, 1992, **139**, 2091–2097.
5 T. Ohzuku and A. Ueda, *J. Electrochem. Soc.*, 1994, **141**, 2972–2977.
6 A. K. Padhi, K. S. Nanjundaswamy and J. B. Goodenough, *J. Electrochem. Soc.*, 1997, **144**, 1188–1194.
7 G.-Z. Wei, X. Lu, F.-S. Ke, L. Huang, J.-T. Li, Z.-X. Wang, Z.-Y. Zhou and S.-G. Sun, *Adv. Mater.*, 2010, **22**, 4364–4367.
8 J. Liu, B. Reeja-Jayan and A. Manthiram, *J. Phys. Chem. C*, 2010, **114**, 9528–9533.
9 A. V. Murugan, T. Muraliganth and A. Manthiram, *Chem. Mater.*, 2009, **21**, 5004–5006.
10 T. Ohzuku and Y. Makimura, *Chem. Lett.*, 2001, **2001**.
11 B. J. Hwang, Y. W. Tsai, D. Carlier and G. Ceder, *Chem. Mater.*, 2003, **15**, 3676–3682.
12 L. Wang, J. Li, X. He, W. Pu, C. Wan and C. Jiang, *J. Solid State Electrochem.*, 2009, **13**, 1157–1164.
13 K. Kang, Y. S. Meng, J. Breger, C. P. Grey and G. Ceder, *Science*, 2006, **311**, 977–980.
14 O. A. Shlyakhtin, Y. S. Yoon, S. H. Choi and Y.-J. Oh, *Electrochim. Acta*, 2004, **50**, 505–509.
15 J. Li, X. He, R. Zhao, C. Wan, C. Jiang, D. Xia and S. Zhang, *J. Power Sources*, 2006, **158**, 524–528.
16 S.-H. Na, H.-S. Kim and S.-I. Moon, *Solid State Ionics*, 2005, **176**, 313–317.
17 S.-T. Myung, K. Izumi, S. Komaba, Y.-K. Sun, H. Yashiro and N. Kumagai, *Chem. Mater.*, 2005, **17**, 3695–3704.
18 G. Y. Kim, *J. Appl. Electrochem.*, 2008, **38**, 1477–1481.
19 R. Guo, P. Shi, X. Cheng and L. Sun, *Electrochim. Acta*, 2009, **54**, 5796–5803.
20 S. Zhang, X. Qiu, Z. He, D. Weng and W. Zhu, *J. Power Sources*, 2006, **153**, 350–353.
21 M. H. Lee, Y. J. Kang, S. T. Myung and Y. K. Sun, *Electrochim. Acta*, 2004, **50**, 939–948.
22 Y. G. Guo, Y. S. Hu, W. Sigle and J. Maier, *Adv. Mater.*, 2007, **19**, 2087–2091.
23 Y. G. Guo, J. S. Hu and L. J. Wan, *Adv. Mater.*, 2008, **20**, 2878–2887.
24 F.-F. Cao, S. Xin, Y.-G. Guo and L.-J. Wan, *Phys. Chem. Chem. Phys.*, 2011, **13**, 2014–2020.
25 F.-F. Cao, Y.-G. Guo and L.-J. Wan, *Energy Environ. Sci.*, 2011, **4**, 1634–1642.
26 F. F. Cao, Y. G. Guo, S. F. Zheng, X. L. Wu, L. Y. Jiang, R. R. Bi, L. J. Wan and J. Maier, *Chem. Mater.*, 2010, **22**, 1908–1914.
27 Y. Yu, L. Gu, C. Wang, A. Dhanabalan, P. A. van Aken and J. Maier, *Angew. Chem., Int. Ed.*, 2009, **48**, 6485–6489.
28 X. L. Wu, L. Y. Jiang, F. F. Cao, Y. G. Guo and L. J. Wan, *Adv. Mater.*, 2009, **21**, 2710–2714.
29 S. Stankovich, D. A. Dikin, G. H. B. Dommett, K. M. Kohlhaas, E. J. Zimney, E. A. Stach, R. D. Piner, S. B. T. Nguyen and R. S. Ruoff, *Nature*, 2006, **442**, 282–286.
30 A. K. Geim and K. S. Novoselov, *Nat. Mater.*, 2007, **6**, 183–191.
31 K. Novoselov, A. Geim, S. Morozov, D. Jiang, Y. Zhang, S. Dubonos, I. Grigorieva and A. Firsov, *Science*, 2004, **306**, 666.
32 F. Ding, H. Ji, Y. Chen, A. Herklotz, K. Dörr, Y. Mei, A. Rastelli and O. G. Schmidt, *Nano Lett.*, 2010, **10**, 3453–3458.
33 C. N. R. Rao, A. K. Sood, K. S. Subrahmanyam and A. Govindaraj, *Angew. Chem., Int. Ed.*, 2009, **48**, 7752–7777.
34 B. Jang and A. Zhamu, *J. Mater. Sci.*, 2008, **43**, 5092–5101.
35 C. Venkateswara Rao, A. Leela Mohana Reddy, Y. Ishikawa and P. M. Ajayan, *ACS Appl. Mater. Interfaces*, 2011, **3**, 2966–2972.
36 H. Wang, Y. Yang, Y. Liang, L.-F. Cui, H. Sanchez Casalongue, Y. Li, G. Hong, Y. Cui and H. Dai, *Angew. Chem., Int. Ed.*, 2011, **50**, 7364–7368.
37 S. Yang, X. Feng, L. Wang, K. Tang, J. Maier and K. Müllen, *Angew. Chem. Int. Ed.*, 2010, **49**, 4795–4799.
38 L. S. Zhang, L. Y. Jiang, H. J. Yan, W. D. Wang, W. Wang, W. G. Song, Y. G. Guo and L. J. Wan, *J. Mater. Chem.*, 2010, **20**, 5462–5467.
39 B. Wang, X.-L. Wu, C.-Y. Shu, Y.-G. Guo and C.-R. Wang, *J. Mater. Chem.*, 2010, **20**, 10661–10664.
40 S. Yang, G. Cui, S. Pang, Q. Cao, U. Kolb, X. Feng, J. Maier and K. Müllen, *ChemSusChem*, 2010, **3**, 236–239.
41 J. Zhu, Y. K. Sharma, Z. Zeng, X. Zhang, M. Srinivasan, S. Mhaisalkar, H. Zhang, H. H. Hng and Q. Yan, *J. Phys. Chem. C*, 2011.
42 H. Wang, L. F. Cui, Y. Yang, H. Sanchez Casalongue, J. T. Robinson, Y. Liang, Y. Cui and H. Dai, *J. Am. Chem. Soc.*, 2010.
43 B. J. Hwang, Y. W. Tsai, C. H. Chen and R. Santhanam, *J. Mater. Chem.*, 2003, **13**, 1962–1968.
44 C. H. Chen, C. J. Wang and B. J. Hwang, *J. Power Sources*, 2005, **146**, 626–629.
45 W. S. Hummers Jr and R. E. Offeman, *J. Am. Chem. Soc.*, 1958, **80**, 1339–1339.
46 J. Xiao, N. A. Chernova and M. S. Whittingham, *Chem. Mater.*, 2008, **20**, 7454–7464.
47 C. J. Wen, B. Boukamp, R. Huggins and W. Weppner, *J. Electrochem. Soc.*, 1979, **126**, 2258.
48 J. Xie, N. Imanishi, T. Matsumura, A. Hirano, Y. Takeda and O. Yamamoto, *Solid State Ionics*, 2008, **179**, 362–370.
49 K. Dokko, M. Mohamedi, M. Umeda and I. Uchida, *J. Electrochem. Soc.*, 2003, **150**, A425–A429.
50 Y. Zhu and C. Wang, *J. Phys. Chem. C*, 2010, **114**, 2830–2841.
51 P. P. Prosini, M. Lisi, D. Zane and M. Pasquali, *Solid State Ionics*, 2002, **148**, 45–51.
52 K. Tang, X. Yu, J. Sun, H. Li and X. Huang, *Electrochim. Acta*, 2011, **56**, 4869–4875.